

**TAMPERE UNIVERSITY OF
TECHNOLOGY
ELECTRONICS LABORATORY**

Tutkimusraportti n:o 4/1984

Research Report No. 4/1984

LOW-COST EDDY-CURRENT MAGNETIC SHIELD
FOR BIOMAGNETIC EXPERIMENTS

J. Malmivuo, J. Leikkala, P. Kontro,
L. Suomaa and H. Vihinen

TAMPEREEN TEKNILLINEN KORKEAKOULU

ELEKTRONIIKAN LABORATORIO

P.O.B. 527 SF-33101 TAMPERE 10

FINLAND



Tutkimusraportti n:o 4/1984

Research Report No. 4/1984

LOW-COST EDDY-CURRENT MAGNETIC SHIELD
FOR BIOMAGNETIC EXPERIMENTS

J. Malmivuo, J. Lekkala, P. Kontro,
L. Suomaa and H. Vihinen

2.7.1984

ISBN 951-720-873-1

LOW-COST EDDY-CURRENT MAGNETIC SHIELD FOR BIOMAGNETIC EXPERIMENTS

J. Malmivuo, J. Lekkala, P. Kontro, L. Suomaa and H. Vihinen

Tampere University of Technology,
Electronics Laboratory,
PO Box 527,
SF-33101 TAMPERE 10, Finland

Abstract

We have constructed a cubic eddy current shield from 45 mm aluminium plate with a 2 m edge. The shield is equipped with an active compensation system to cancel the static and low-frequency magnetic field. The performance of the shield and the compensation system is measured very accurately. These measurements and the measurement of biomagnetic fields show that eddy-current shielding is a practical solution for clinical biomagnetic measurements because of its low cost and the small space it needs.

CONTENTS

1. INTRODUCTION	1
2. REQUIRED SHIELDING	3
3. EDDY CURRENT SHIELDING	6
3.1. Theory	6
3.2. Construction	6
3.3. Attenuation	8
4. ACTIVE DC COMPENSATION SYSTEM	9
4.1. Requirements for DC compensation	9
4.2. Coil system	10
4.2.1. Design of the coil system	10
4.2.2. Mathematical calculations	11
4.2.3. The constructed coil sets	13
4.3. Power source	17
4.3.1. Construction of the current source	18
4.3.2. Noise properties	19
4.4. Compensation field distribution	19
4.4.1. Measurement equipment	20
4.4.2. Measurements	21
4.4.3. Results	22
5. ACTIVE AC COMPENSATION SYSTEM	26
5.1. Requirements for the AC compensation	26
5.2. Transducer coils	27
5.3. Alternating field compensator	28
5.4. Performance of the AC compensation system	31
6. PERFORMANCE OF THE TAMPERE MAGNETICALLY SHIELDED ROOM IN BIOMAGNETIC EXPERIMENTS	33
7. DISCUSSION	36
8. SUMMARY	37
REFERENCES	39

1. INTRODUCTION

Research on biomagnetic phenomena has become so popular that more than 30 laboratories are at present active in this field [Rom 82]. The low level of biomagnetic signals involves the use of very sensitive SQUID instrumentation and effective magnetic noise rejection.

The magnetic noise can be attenuated in the following ways:

- elimination of the magnetic noise source
- appropriate detector design (gradiometer)
- passive magnetic shielding (μ -metal or eddy-current shield)
- active compensation of the noise field.

The best result is obtained with an appropriate combination of these methods.

It is possible to effect passive magnetic shielding with a multi-layer magnetically permeable shield or with a thick-walled eddy-current shield. The ferromagnetic shield was first proposed for biomagnetic studies by Safonov [Saf 67] and Cohen [Coh 67]. The multilayer ferromagnetic shield, possibly together with an eddy-current shield, is very effective and is used in several laboratories [Wik 75, Kel 82, Mag 81, Ern 81]. Also pure eddy-current shields have been constructed for biomagnetic measurements [Zim 77, Ber 81, Str 81]. The price of the μ -metal shield is several hundred thousand dollars in addition to the structural changes to the surrounding building. However, it is possible to place the pure eddy-current shield in a normal laboratory room and its price is in the range of ten thousand dollars.

The purpose of this paper is to show, on the basis of our measurements of the performance of the eddy-current shield of Tampere University of Technology, that a carefully designed eddy-current shield with an appropriate active compensation system is a cheap and adequate solution for biomagnetic measurements, not only, for research laboratories but especially for clinical use.

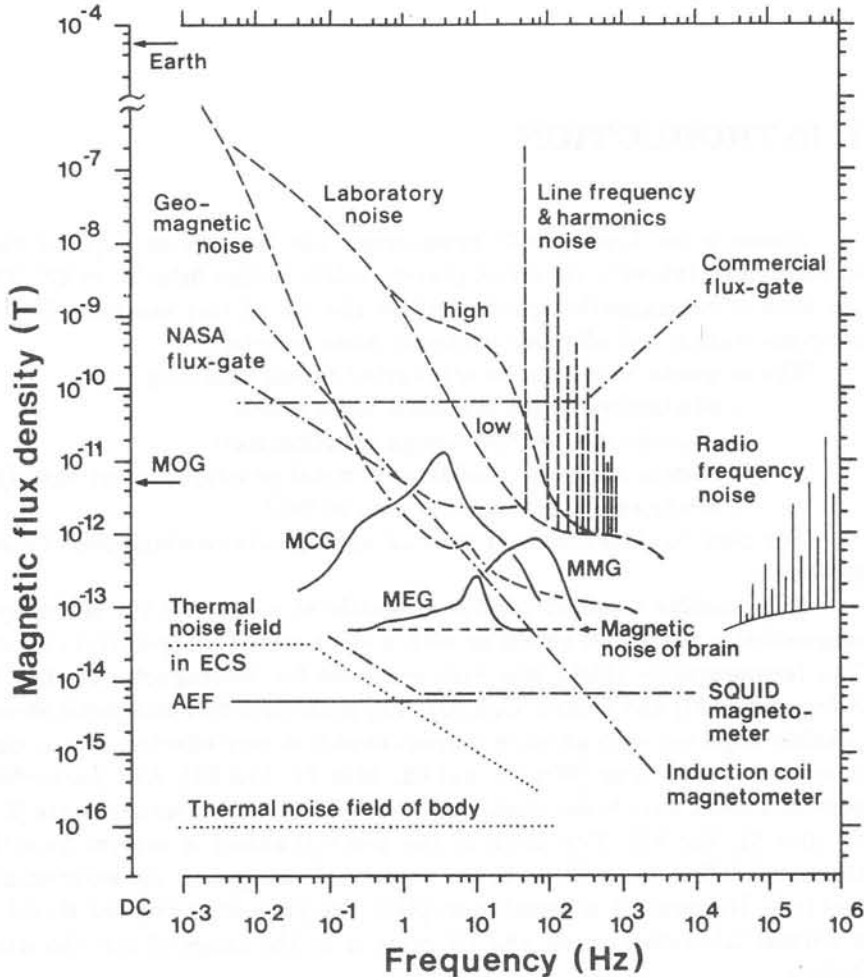


Figure 1. Spectral density of the magnetic fields generated by different sources. Biomagnetic signals: magnetocardiogram (MCG), magnetomyogram (MMG), magnetoencephalogram (MEG), magneto-oculogram (MOG) and auditory evoked fields of brain (AEF). Noise fields: DC field of earth, geomagnetic fluctuations, man-made noise in a laboratory, field components on the line frequency and its harmonics, and radio-frequency interferences. The thermal noise fields are shown in two cases; the field inside an eddy current shield (ECS) and the field in the vicinity of a human body. The equivalent input magnetic noise of three types of magnetometers as a function of frequency: commercial flux-gate magnetometer, ring-core flux-gate magnetometer of NASA, induction coil magnetometer and SQUID magnetometer.

2. REQUIRED SHIELDING

The spectra of the most important biomagnetic signals and magnetic noise fields are summarized in Fig. 1. The figure shows also the sensitivity of a typical commercial SQUID-magnetometer. It may be seen from the figure that the dominating noise source is the magnetic noise from electric appliances and movements of ferromagnetic particles in the earth's static field, which is called the laboratory noise. Therefore, careful selection of the laboratory location makes an important improvement in the biomagnetic signal quality.

The high intensity of the line frequency noise is worth mentioning. The satisfactory condition for the functioning of a SQUID-magnetometer is that the externally coupled noise field does not exceed the maximum slew-rate of the flux-locked loop. This together with the gradiometer type used determines the maximum acceptable noise level in the experimental area. The line frequency noise can be reduced using a *5-lead* system in the electric installation of the laboratory surroundings. The remaining line frequency noise and its harmonics in the measured signal are easy to filter with a digital comb filter and therefore these are not dominating factors in determining the required amount of shielding.

The frequency of the radio frequency (RF) magnetic noise is so high, that it can be easily eliminated with a thin aluminium foil around the measurement detector or the Dewar. The RF-fields are also attenuated to an insignificant level by using a door in the shielded chamber. A thin well-conducting plate with small holes or even a metalwire-netting door is sufficient.

According to the aforementioned text, the required shielding factor may be determined on the basis of the existing laboratory noise. A practical limit for the shielding is the noise level of the detector. At the moment, the noise level of a commercial RF-SQUID equipment unit is in the range $50 - 20 fT_{rms}/\sqrt{Hz}$ in the frequency band from a few hertz to a few kilohertz. However, it is expected that the noise level will be decreased with about one decade when the DC-SQUIDS become more common.

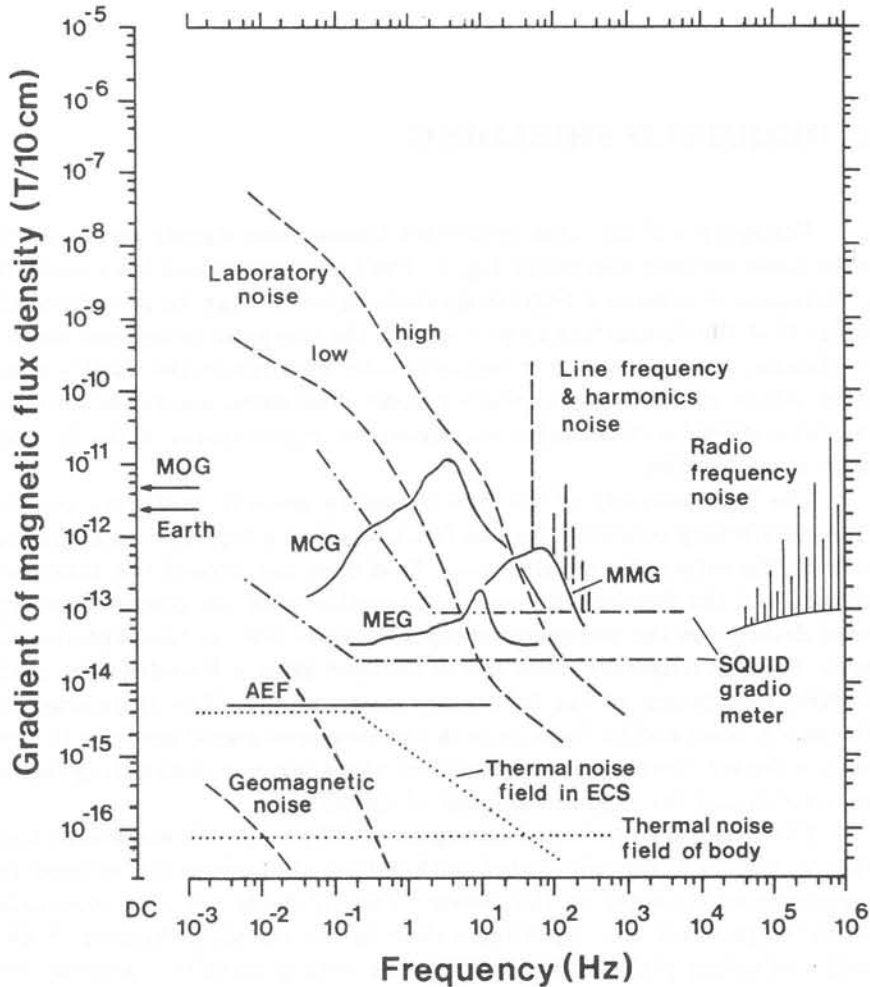


Figure 2. Spectral density of the magnetic field gradients generated by different sources (gradiometer baseline 10 cm). Biomagnetic signals: magnetocardiogram (MCG), magnetomyogram (MMG), magnetoencephalogram (MEG), magneto-oculogram (MOG) and auditory evoked field of brain (AEF). Noise fields: DC field gradient of earth, geomagnetic fluctuations, laboratory noise (calculated from the field of Fig. 1 with different types of sources), line frequency noise and radio-frequency noise. Thermal noise field gradients in an eddy current shield (ECS) and near to a human body are shown. The equivalent magnetic gradient noise of two typical SQUID gradiometers is presented.

In the frequency range over 1 Hz, the magnetocardiogram signal is typically 40-80 dB under the laboratory noise level in the worst case, Fig. 1. The corresponding figure for magnetoencephalography is 60-80 dB. To achieve a signal-to-noise ratio of 30 dB, which is a very good value, an attenuation of the noise fields of 70-90 dB and 90-110 dB, respectively, is needed.

However, the magnetometer is easy to construct as a differential magnetometer or gradiometer of the first, second or even higher order. The gradiometric detector coil decreases the needed attenuation of the shield considerably. The second and higher order gradiometers make it possible to use them in some cases even without any external shielding in a normal laboratory [Wil 81]. Figure 2 shows the magnetic field gradient of the signals of Fig. 1 measured with a gradiometer with a 10 cm baseline. This figure shows that because a gradiometer is nowadays used as a magnetic field detector the ultimate shielding requirements are much smaller than Fig. 1 would predict.

3. EDDY CURRENT SHIELDING

Zimmerman has described a method of constructing the magnetically shielded enclosure from thick-walled conducting material [Zim 77]. The benefits of its use are low price and easy and rigid construction. Its main disadvantage is that the attenuation provided by the shield is a linear function of frequency and is zero for a static field.

3.1. Theory

Zimmerman approximates the shield with a long rectangular tube and calculates the field strength H inside the shield for an external field strength H_{ex} to be

$$H(\omega) = \frac{H_{ex}(\omega)}{(1 + j\omega\tau)} \quad (1)$$

where

$$\tau = \frac{\mu_o \sigma w h t}{2(w + h)} \quad (2)$$

and

- ω = angular frequency,
- σ = the conductivity of the material,
- h = the height of the shield,
- w = the width of the shield,
- t = the wall thickness.

The time constant τ characterises the response to a uniform applied field.

3.2. Construction

The shield is constructed from 45 mm thick aluminium plate and has the outer dimensions $2\text{m} \times 2\text{m} \times 2\text{m}$, Fig. 3. The doorway is constructed as a short corridor to enhance the attenuation in the z -direction. The aluminium has the purity of 99.5% with a conductivity of $3.6 \cdot 10^7$ S/m. The shield weighs approximately 3000 kg.

To avoid the interference induced through the vibration of the detector in the earth's static field, the shield is equipped with pneumatic dampers. These insulate the vibrations of the floor. Additionally, the

shield is equipped with a plywood floor which is fixed with brass rods to the laboratory floor. Otherwise the patient's heartbeats would induce considerable noise through the movement of the shield.

The dimensions of the Biomagnetic Laboratory where the shield is are of the order of a normal laboratory room, $3\text{m} \times 6\text{m} \times 6\text{m}$. In the laboratory the following specific structural procedures have been accomplished. The floor of the laboratory is disconnected from the walls and lies on a sandmattress. This attenuates the vibration of the building in the measurement area. The concrete of the floor is reinforced with steel which contains more carbon than normally and thus its permeability, which tends to distort the static field distribution, is lower. The electricity at the ceiling lights is led straight through the ceiling and not along it. This attenuates the line frequency components. The heating radiators made from heavy iron produced considerable noise and were changed to ones made of copper.

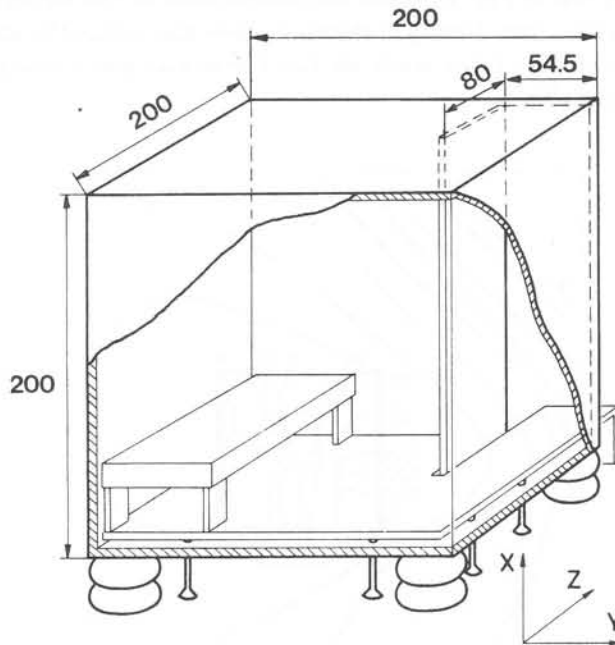


Figure 3. Construction of the Tampere magnetically shielded room. This eddy current shield is made from 45mm thick aluminium plate. The shield is equipped with pneumatic dampers to insulate against the vibrations of the laboratory floor. The magnetometer is mounted on the inner wall of the shield and for the patient there is a bed on a plywood floor. This additional floor is fixed with brass rods to the laboratory floor. Dimensions given in cm.

3.3. Attenuation

Theoretically, calculated from Eqs. (1) and (2), when the conductivity of the aluminium wall is $3.6 \cdot 10^7$ S/m, its thickness is 0.045 m and the dimensions of the enclosure are $2\text{m} \times 2\text{m} \times 2\text{m}$, the time constant τ equals 1.02 s and the attenuation is 50 dB at 50 Hz. This value of attenuation applies for a closed shield without door.

The measured attenuation of the shield to the 50 Hz magnetic field in the laboratory is described previously [Hei 80, Mal 81]. To summarize the previous results, we would mention that the theoretically predicted 50 dB attenuation is achieved in the z-direction. In the y-direction the attenuation is 46 dB and in the x-direction (vertical direction), due to the doorway, the smallest, 44 dB. An example of the attenuation properties of the shield is shown in Fig. 4, where the distribution of the z-component of the 50 Hz magnetic flux density is shown outside and inside the shield. The measurements of Fig. 4 are made on the horizontal plane going through the center of the shield.

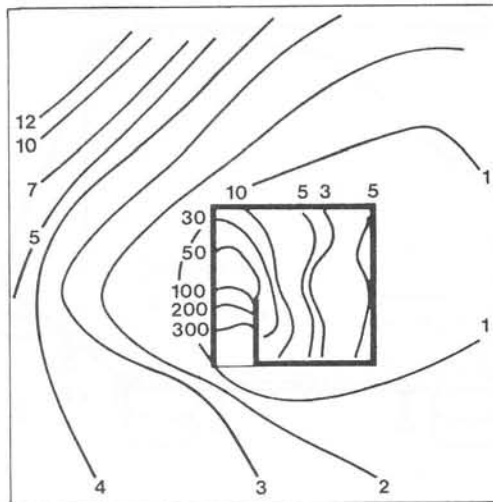


Figure 4. RMS values of the z-component of the 50 Hz magnetic flux density in the laboratory outside and inside the shield. The dimensions are in nT outside the shield and in pT inside the shield.

4. ACTIVE DC COMPENSATION SYSTEM

The eddy-current shield is equipped with an active compensation system to compensate for the earth's static magnetic field. The system includes three mutually perpendicular sets of coils in the laboratory and a high quality power source.

4.1. Requirements for DC compensation

The steady magnetic field does not itself cause distortion when low level alternating magnetic fields are measured. The noise is, however, induced to the pick-up coil when it is subject to mechanical vibrations in the static field. While the steady magnetic field is comparatively homogeneous, little of the noise is caused when the pick-up coil is vibrating in the direction of its axis. Most of the noise is caused when the pick-up coil tilts in

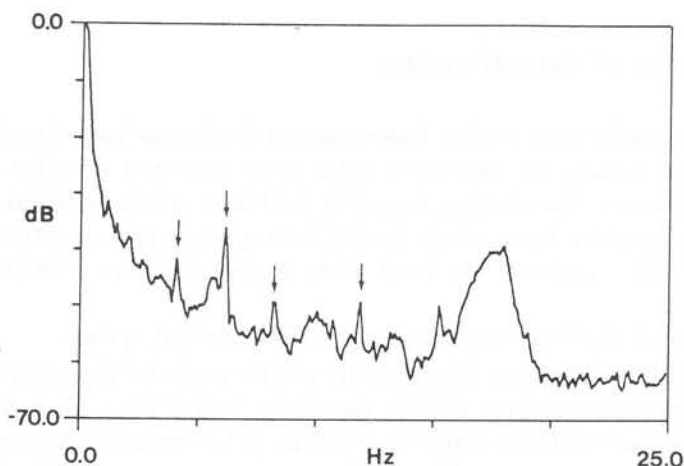


Figure 5. Spectrum of the magnetic noise of an induction coil magnetometer in the z -direction. The spikes of the spectrum pointed out by arrows are due to the alternating fields. The broader ones are caused by the mechanical vibrations.

the static field. In Fig. 5 the spectrum of the noise induced to a detection coil has been presented. The sharp spikes of the spectrum, which are pointed out by arrows, are due to the alternating fields, and the broader ones are caused by the mechanical vibration. The other cause of noise in the static magnetic field is when a ferromagnetic particle is moving in the field and disturbs its homogeneity.

In magnetic cardiac studies, when an external magnetic field affects the thorax, a susceptibility signal is generated. It is due to the changes in the intracardiac blood volume which change the susceptibility of the thorax. Also the movement of the heart muscle and the surrounding tissue contribute to the susceptibility signal [Kat 82].

The static magnetic field of the earth should thus be compensated for as well as possible. However, if there is not used a transducer for detecting the low-frequency fluctuations of the field (low frequency AC compensation), but the compensation current setting is fixed and made once before measurements, it is enough that the field is attenuated to the level of the geomagnetic and other low frequency fluctuations.

4.2. Coil system

4.2.1. Design of the coil system

Theoretically, remarkably homogeneous fields over large fractions of the enclosed volume are realizable with ideal multi-coil sets [Pit 63]. In practice, however, the existing magnetic field is so inhomogeneous that it is not necessary to achieve a high level of homogeneity in the compensating magnetic field. Then also the positioning accuracy of the coils is not so critical.

We stated the following requirements for our coil system:

- 1) The calculated homogeneity of the magnetic field in the compensated central volume should be better than 10^{-4} within a sphere with the diameter of 0.6 m. (The concept of homogeneity is defined later in Eq. 4). However, it is very probable that the pre-existing gradients are greater than this homogeneity [Fre 67].
- 2) It is easy to fit in the laboratory and in the space it compensates for.
- 3) It is easy to make the coils.

The general configuration of the current loops designed to generate homogeneous fields is characterized by two types of symmetry [Bre 69]:

- the coils are symmetric in relation to the axial point and
- the coils are located on a common axis symmetrically in relation to the origin.

A coil set is called symmetric if the current direction is the same in the two coils that form a symmetric pair; otherwise it is called antisymmetric. If the coil set is symmetric, all odd derivatives of the field at the origin are zero [Bre 69]. In order to obtain a homogeneous field it is thus necessary to eliminate only even derivatives of higher order. With a coil set of n coils one can eliminate $n-1$ derivatives. The derivatives higher than the sixth order have no essential effect on the field homogeneity in the space around the origin.

4.2.2. Mathematical calculations

The magnetic field strength H along the axis of a symmetric system of circular or square coils can be written in the form [Pit 63, Kak 76]

$$H = \sum_{n=0}^{\infty} a_{2n} z^{2n} \quad , \quad (3)$$

where z = the distance from the origin,
 a_{2n} = the source term.

To achieve a highly homogeneous magnetic field it is necessary to eliminate as many of the successive higher order terms beyond a_0 as possible.

Magnetic fields produced by different coil sets are compared by means of the inhomogeneity of the field on the axis of the coil set. The field inhomogeneity E is given by the relation [Bre 69]

$$E = 1 - \frac{H(x)}{H(0)} \quad , \quad (4)$$

where $H(x)$ = the field at the axial point,
 $H(0)$ = the field at the origin.

For thin circular current loops as in Fig. 6a one can calculate the magnetic field in terms of the complete elliptic integrals $K(k)$ and $E(k)$ as follows [Web 54]

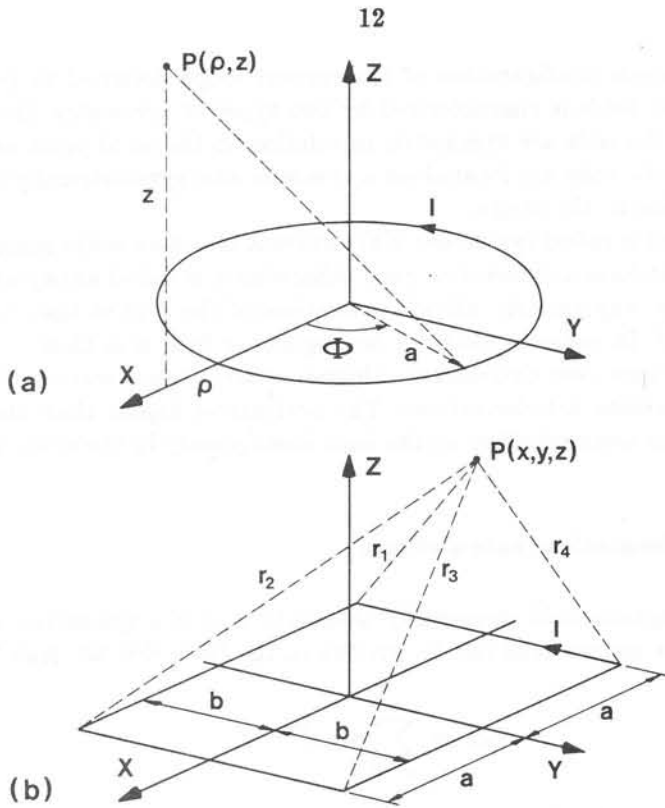


Figure 6. Geometry for calculation of the magnetic field at point P produced by a thin circular current loop (a) and a rectangular current loop (b).

$$B_{\rho} = \frac{\mu}{2\pi} I \frac{z}{\rho} [(\rho + a)^2 + z^2]^{-1/2} \left[-K(k) + \frac{a^2 + \rho^2 + z^2}{(a - \rho)^2 + z^2} E(k) \right], \quad (5)$$

$$B_z = \frac{\mu}{2\pi} I [(\rho + a)^2 + z^2]^{-1/2} \left[K(k) + \frac{a^2 - \rho^2 - z^2}{(a - \rho)^2 + z^2} E(k) \right], \quad (6)$$

$$B_{\Phi} = 0, \quad (7)$$

where

$$k^2 = \frac{4\rho a}{(\rho + a)^2 + z^2}.$$

Similarly for rectangular loops as in Fig. 6b one can calculate the magnetic field as follows [Web 54]

$$B_x = \frac{\mu I}{4\pi} \sum_{i=1}^4 (-1)^{i+1} \frac{z}{r_i(r_i + y_i)} \quad , \quad (8)$$

$$B_y = \frac{\mu I}{4\pi} \sum_{i=1}^4 (-1)^{i+1} \frac{z}{r_i(r_i + x_i)} \quad , \quad (9)$$

$$B_z = \frac{\mu I}{4\pi} \sum_{i=1}^4 (-1)^i \frac{r_i(x_i + y_i) + x_i^2 + y_i^2}{r_i(r_i + x_i)(r_i + y_i)} \quad , \quad (10)$$

with

$$\begin{aligned} x_1 &= x_4 = x + a \\ x_2 &= x_3 = x - a \\ y_1 &= y_2 = y + b \\ y_3 &= y_4 = y - b. \end{aligned}$$

4.2.3. The constructed coil sets

Rectangular coils were chosen because they are easier to make than circular coils and they occupy less of the working volume in the laboratory. The homogeneity of the magnetic field produced by square coils or rectangular coils is essentially as good as the homogeneity of the field due to the corresponding inscribed circular coils, as can be seen from Fig. 7.

The vertical or x-component of the magnetic field is compensated for with four coaxial square coils in two planes. Thus the doorways are not closed with the coils. The y- and z-components are each compensated for with four coaxial rectangular coils in four planes. Such coils occupy as little as possible of the working volume in the laboratory, Fig. 8. The dimensions and the ampere-turns of the coils are summarized in Table 1. The dimensions of the x coils have been solved according to the method of *Kakuno* and *Gondo* [Kak 76], and the dimensions of the rectangular coils in the y- and z-directions experimentally on the basis of the square coil solution. We do not claim that the rectangular solution is the optimum solution.

The coils in each coil set are connected in series. Each coil set consists of two pairs of coils. The effect of the second coil pairs on the homogeneity is presented in Table 2. In Table 3 we have summarized the theoretical field homogeneities for the complete 2-coil pair sets (x- and y-sets) calculated at some points in the compensated central volume around the origin. The vertical and horizontal components of the static magnetic field of the earth at Tampere are 55 μT and 16 μT , respectively. They can be compensated

for with the ampere-turns presented in Table 1.

The larger and smaller x-coils have 82 and 2 turns, respectively. Thus a current of 2 amperes is needed to compensate for the vertical component. The resistance of the four x-coils connected in series is 20 ohms. The y- and z-coils have 10 and 28 turns, respectively. Thus the maximum current of 1 ampere is needed to compensate for the horizontal component that is the resultant of the y- and z-components. The total resistance of the y- or z-coils is 27 ohms.

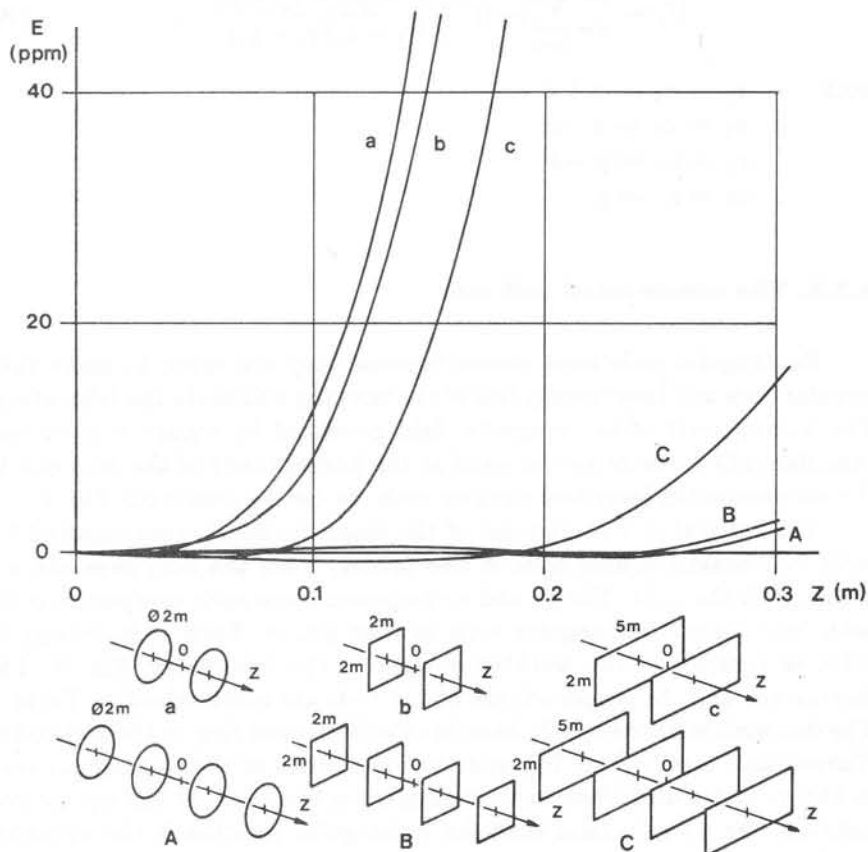


Figure 7. Inhomogeneity of the magnetic field produced by different coil sets. Lower case letters are used for the two-coil systems and upper case letters for the four-coil systems. A-curves: circular coils with 2 m diameter, B-curves: square coils with 2 m side and C-curves: 2 m \times 5 m rectangular coils. Z is the distance from the origin along the axis of the coil set.

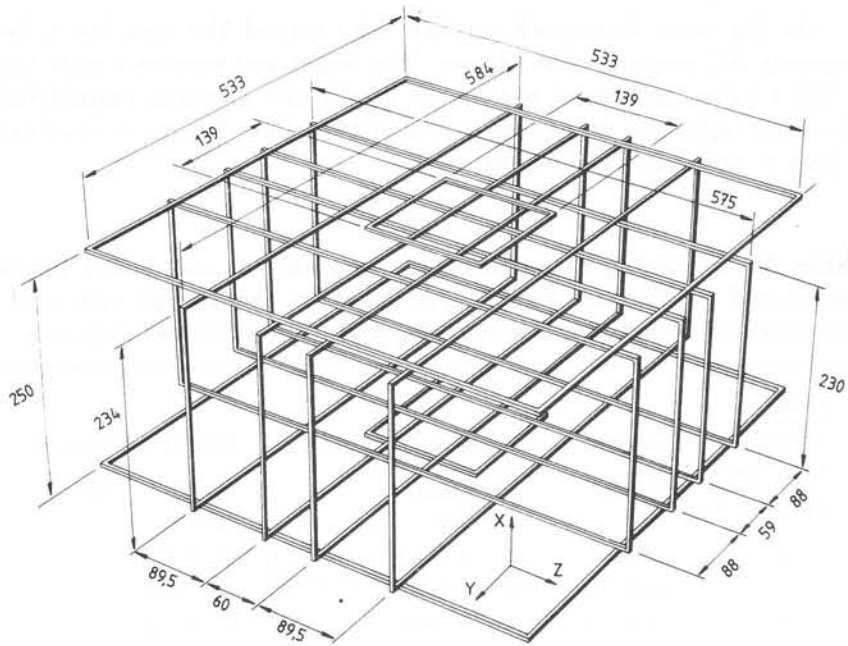


Figure 8. Constructed compensation coil set for the x-, y- and z-directions. Dimensions given in cm.

Table 1. Dimensions and ampere-turns of the coil sets.

COIL SET	COIL DIMENSIONS [m]	COIL DISTANCE FROM ORIGIN [m]	AMPERE TURNS
X	5.33 x 5.33	+ 1.25	164
	5.33 x 5.33	- 1.25	164
	1.39 x 1.39	+ 1.25	4
	1.39 x 1.39	- 1.25	4
Y	2.30 x 5.75	+ 0.295	10
	2.30 x 5.75	- 0.295	10
	2.30 x 5.75	+ 1.175	28
	2.30 x 5.75	- 1.175	28
Z	2.34 x 5.84	+ 0.300	10
	2.34 x 5.84	- 0.300	10
	2.34 x 5.84	+ 1.195	28
	2.34 x 5.84	- 1.195	28

On the same framework we have also wound the coils for a low-frequency AC compensation system. The larger and smaller x-coils have 41 and 1 turns, and the y- and z-coils have 5 and 14 turns, respectively. The series resistance of the four x-coils is 430 ohms. The series resistance of both y- or z-coils is 150 ohms.

Table 2. Calculated magnetic field along the x- and y-axis for the constructed x-coils and y-coils. The effect of the second coil pair is demonstrated separately. The inhomogeneity E is expressed in ppm's.

X COILS						
DISTANCE FROM THE ORIGIN [m]	LARGER COILS		SMALLER COILS		COMPLETE COIL SET	
	FIELD [μT]	E	FIELD [μT]	E	FIELD [μT]	E
0.00	54.2213	0	0.9582	0	55.1795	0
0.04	54.2185	50	0.9692	$-1.1 \cdot 10^4$	55.1795	0
0.08	54.2104	200	0.9690	$-1.1 \cdot 10^4$	55.1794	0
0.12	54.1967	450	0.9827	$-2.6 \cdot 10^4$	55.1793	0
0.16	54.1773	810	1.0019	$-4.5 \cdot 10^4$	55.1792	10
0.20	54.1522	1270	1.0268	$-7.1 \cdot 10^4$	55.1790	10
0.24	54.1212	1850	1.0576	$-1.0 \cdot 10^5$	55.1788	10
0.28	54.0839	2530	1.0946	$-1.4 \cdot 10^5$	55.1785	20

Y COILS						
DISTANCE FROM THE ORIGIN [m]	INNER COILS		OUTER COILS		COMPLETE COIL SET	
	FIELD [μT]	E	FIELD [μT]	E	FIELD [μT]	E
0.00	7.0527	0	10.5931	0	17.6457	0
0.04	7.0469	820	10.5989	-550	17.6457	0
0.08	7.0296	3280	10.6162	-2180	17.6458	0
0.12	7.0008	7350	10.6450	-4900	17.6458	0
0.16	6.9608	13030	10.6849	-8670	17.6457	0
0.20	6.9097	20260	10.7358	-13470	17.6456	10
0.24	6.8480	29020	10.7973	-19280	17.6453	30
0.28	6.7759	39240	10.8689	-26030	17.6448	60

Table 3. Inhomogeneity of the field calculated at some points in the central volume for the constructed complete set of x-coils and y-coils. The inhomogeneity E is expressed in ppm's.

X COILS	Y,Z [m]	E						
		0.00	0.05	0.10	0.15	0.20	0.25	0.30
X [m]								
0.00		0	0	0	- 10	- 20	- 40	- 70
0.04		0	0	0	- 10	- 20	- 40	- 70
0.08		0	0	0	- 10	- 20	- 40	- 80
0.12		0	0	0	- 10	- 20	- 40	- 80
0.16		10	0	0	- 10	- 20	- 40	- 80
0.20		10	10	0	0	- 20	- 40	- 90
0.24		10	10	10	0	- 20	- 40	- 90
0.28		20	20	10	0	- 10	- 40	- 90

Y COILS	X,Z [m]	E						
		0.00	0.05	0.10	0.15	0.20	0.25	0.30
Y [m]								
0.00		0	0	0	10	30	60	120
0.04		0	0	0	10	20	60	110
0.08		0	0	0	0	10	30	80
0.12		0	0	- 10	- 10	- 10	0	30
0.16		0	0	- 10	- 30	- 40	- 40	- 30
0.20		10	0	- 20	- 40	- 70	- 90	-100
0.24		30	20	- 10	- 50	-100	-150	-180
0.28		60	40	0	- 60	-140	-210	-260

4.3. Power source

To compensate for the earth's magnetic field with the coil set, three independent current sources are needed. The values of the currents in all compensation coils have to be exactly adjustable and the adjustments have to remain when the device is switched off. When a current through an inductive load is switched on or off, a high voltage transient is produced. The device is protected carefully against this.

The coupling of line frequency interference to the compensation current has to be prevented carefully so that its effect in the measurement area is clearly below the externally coupled magnetic line frequency noise. In addition, the thermal drift of the current source should cause less change in the magnetic field than the externally coupled magnetic fluctuations.

4.3.1. Construction of the current source

Figure 9 presents the circuit diagram of the current feeding system. The operational amplifier *OA* drives VMOSFET *Q* and keeps with negative feedback the voltage over the resistor R_s constant. As the voltage over R_s stays stable, the current through compensation coil *L* will be stable as well. The reference voltage is adjusted by potentiometers P_1 and P_2 . The diode *D* protects the transistor from voltages with opposite polarity when the device is turned on and off. The high voltage transients existing during the switching are eliminated by forcing the voltage over the load to vary slowly, having a time constant of the order of 2 s.

All three channels have been constructed on the same principle. The component values are selected so that the y- and z-channels can feed current up to 1 A, and x-channel up to 2 A. Vernier adjustment arranged by potentiometer P_2 can set currents at an accuracy of 0.1 mA on the y- and z-channels and of 0.2 mA on the x-channel.

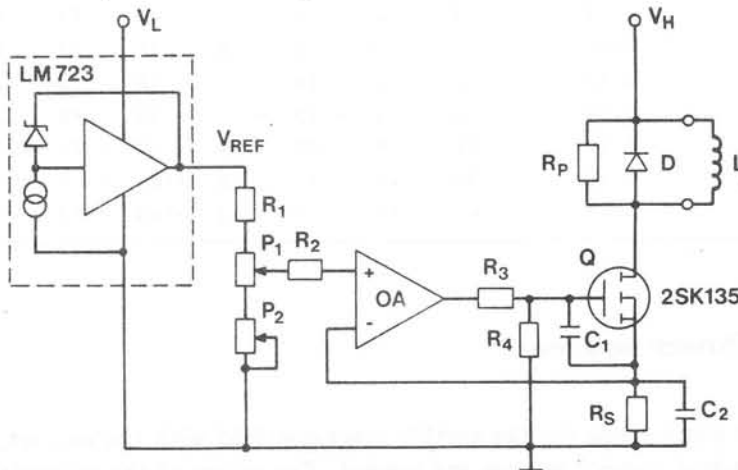


Figure 9. Current feeding unit for the DC compensation system.

4.3.2. Noise properties

Table 4 lists the line frequency and its harmonic components in the steady field compensation current. Each channel was loaded with the theoretical current values which are needed for the elimination of the earth's steady field. The thermal drift of the current causes changes in the steady magnetic field. During the first hour after switching on the compensator the drift was in the x-, y- and z-channels 900 μA , 300 μA and 600 μA , respectively. This corresponds approximately to a 27 nT change in the total flux density. After one hour's warmup time all the three channels were quite stable. The change in the current of the x-channel was less than 160 μA , and that of the y- and z-channels less than 80 μA during a day. This causes a 4.8 nT drift in the total magnetic flux density. As the earth's static field fluctuates maximally 30 nT - 100 nT, the thermal drift of the source will clearly produce less changes in the static field.

4.4. Compensation field distribution

The field distribution of the DC compensation coil set was tested by measuring the magnetic field gradient between the center of the coils and a field point when an appropriate current was fed to the coils. The measurements were performed with a flux-gate magnetometer (Förster). The straightforward DC measurement was not possible with the accuracy desired ($\pm 1\text{nT}$), because of the fluctuations of the order of 100 nT/day in the earth's magnetic field. Also the flux-gate magnetometer is most sensitive as a nullindicator, because it is DC-coupled and its sensitivity is thus inversely proportional to the absolute value of the field to be measured.

Table 4. Amplitude of the line frequency and its harmonic components in the steady compensation current. Each channel was loaded by the current which is needed for the elimination of the earth's field.

	f [Hz]	X	Y	Z
I_{dc} [mA]	0	1560	697	484
	50	32.4	15.4	12.2
I_{ac} [μA]	100	1.4	0.3	0.3
	150	49.1	32.5	28.9

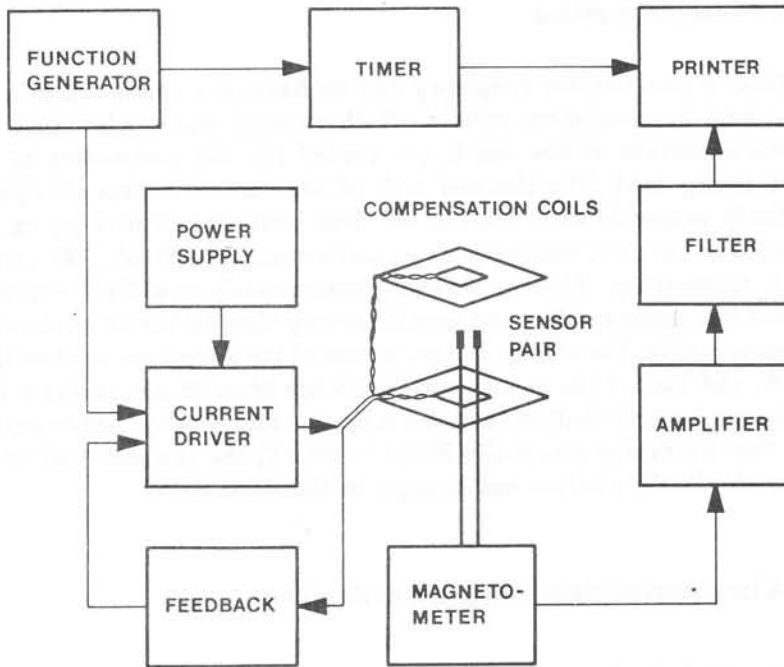


Figure 10. Block diagram of the DC field measurement system. The magnetometer is a commercial flux-gate magnetometer (Förster).

The effect of the geomagnetic fluctuations was avoided by feeding a square wave current to the coils and measuring the peak-to-peak value of the magnetic field at each point. This method was independent of the low-frequency fluctuations. The properties of each of the three compensation coil sets x, y and z were measured separately and thus the current was fed only to the coil set under examination. The higher limit to the frequency of the input square wave current was determined by the time-constant of the magnetically shielded room (measured to be $\tau = 0.85$ s) and the low-pass filters used. The limit to the lowest usable frequency was determined by the highest frequencies of the magnetic field fluctuations. The chosen frequency for the input square wave current was 0.05 Hz.

4.4.1. Measurement equipment

The block diagram of the measurement system is shown in Figure 10. The function generator drives both the current feeding system and the timing unit which controls the printer. The construction of the cur-

rent feeding unit is the same as in the aforementioned DC compensation current source. The magnetometer measures the field gradient between the origin and the given measurement point. Thus the measurement result is proportional to the inhomogeneity. The output of the magnetometer is fed through filters to the input of the printer. The final value of the field gradient, ΔB , is the averaged peak-to-peak value of the square wave from which a total of eight samples were taken.

For adjustments of the sensors a sensor holder was constructed from aluminium and brass. The holder was fixed to the inner walls of the magnetically shielded room. The measurement sensor was fixed to the movable construction. It consisted of two rods, the horizontally positioned main rod and the vertically positioned support rod, which moved on the main rod. It was possible to measure on one xz -plane all three components of the field at a time. The reference sensor was fixed to a firm aluminium rod, which was suspended from the roof of the shield so that the sensor was in the origin of the coil set.

The measurement grid increment was selected to be 15 cm. The dimensions of the grid were the following:

x: -75cm - +75cm
 y: -30cm - +75cm
 z: -75cm - +75cm

Measured points per each component were $8 \times 11 \times 11 = 968$ and thus a total of 2904. The volume examined was 2.36 m^3 . A fully cubic grid was not possible because of the corridor wall in the positive y -direction.

4.4.2. Measurements

Before starting the measurements all material containing iron, such as tables, chairs and electrical equipment, were removed from the laboratory. The measurement instruments were located in the room's corner as far from the measurement location as possible. The magnetically shielded room was earthed during the measurements. The pneumatic dampers were not used because the coordinates of the sensor-holder construction were fixed to the shield.

The measurements were carried out mostly during weekends and during the evenings and nights of weekdays. Then the disturbance level in the laboratory was smallest. It took about a week and a half to measure one component. The sensors used were very sensitive to deflections of their position. So the orientation of the sensors were checked with a level before the measurement of every new plane.

The measurements were performed one component at a time. The grid

was gone through plane by plane. At each point of the plane three field difference measurements were made, one for each component. Before and after the daily measurement process also the flux density measurements were made to compare the values measured on different days. To reach better measurement accuracy the feeding currents were maximized. The upper limit for the current value was the biggest allowable coil current and the biggest output voltage of the current source. Thus the feeding currents were much higher than those used for compensation of the earth's field. The multiplication factors for x-, y- and z-currents were 1.78, 3.33 and 5.33, respectively, when compared to the compensation currents. The measured values were fed to a VAX 11/780 computer for analysis.

4.4.3. Results

In Fig. 11 the calculated theoretical distribution of the DC compensation flux density in the x-direction on the yz-plane is shown. The region on which the measurements have been made is marked with the thick line at the top of the distribution. Figs. 12a, 12b and 12c show as pseudo three-dimensional pictures the calculated and measured inhomogeneities on the three perpendicular planes generated by the DC field compensation coil set in the x-, y- and z-direction, respectively.

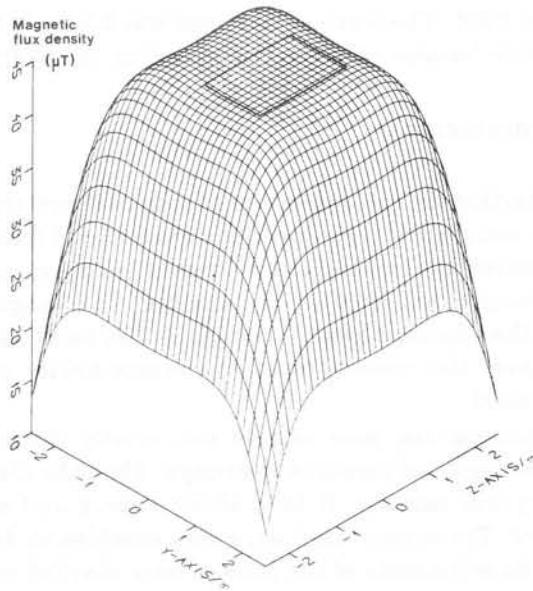


Figure 11. Calculated theoretical distribution of the magnetic flux density in the x-direction on the yz-plane ($x = 0$ cm) produced by the x-compensation coil set.

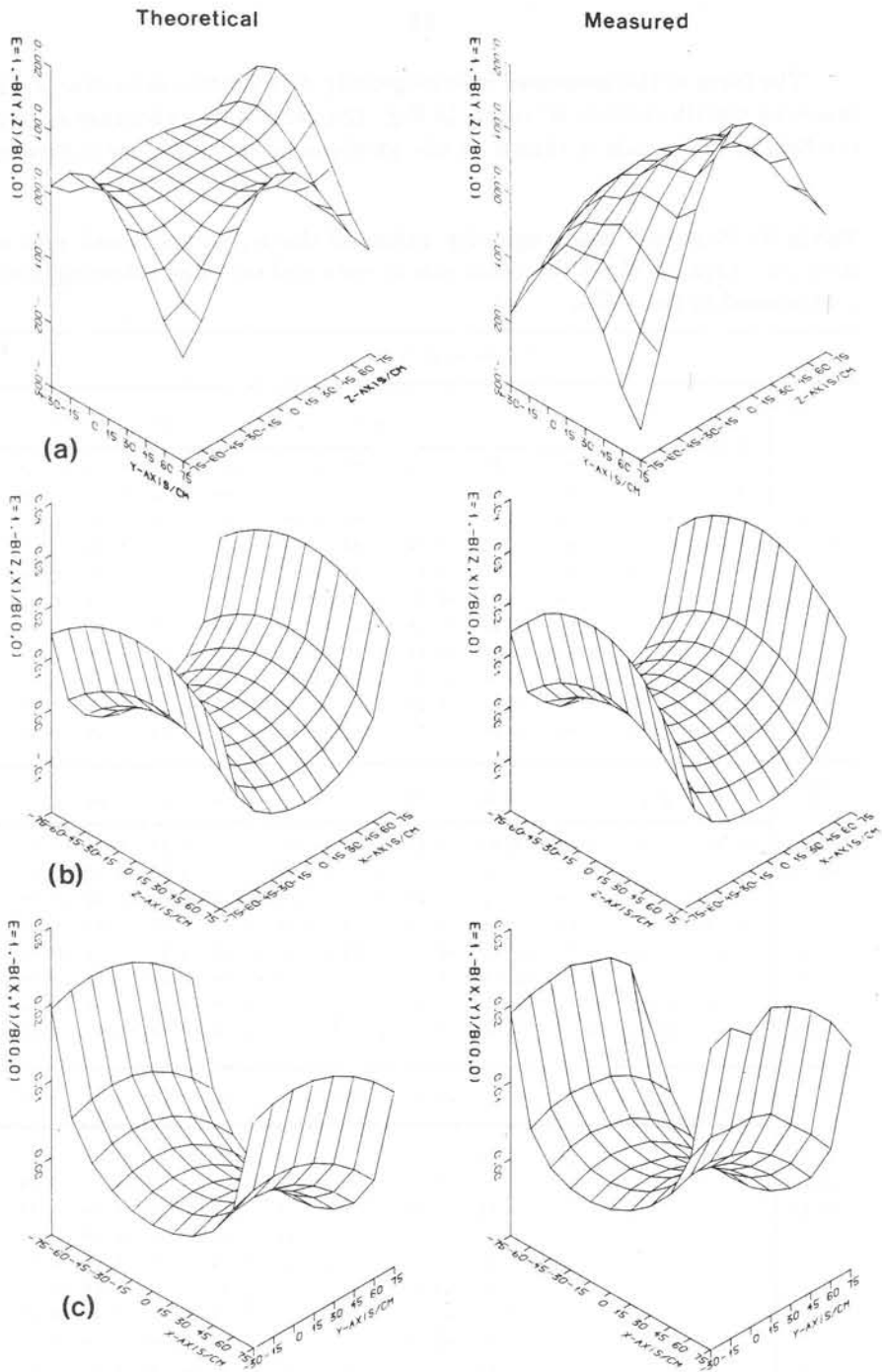


Figure 12. Theoretical and measured inhomogeneity values of the field of the three compensation coil sets on three orthogonal planes. (a) x-coils, (b) y-coils and (c) z-coils.

The form of the measured inhomogeneity distribution is similar to the theoretic distribution in all cases. In Fig. 12a, where the inhomogeneity of the field of the x-coils is shown on the yz-plane ($x = 0$ cm), the difference

Table 5. Measured inhomogeneity values of the x-, y- and z-coil sets on the plane directed along the main axis of each coil set. The inhomogeneity is expressed in per mills.

		Inhomogeneity E[‰]										
$Y=0,$ Z		-0.75	-0.60	-0.45	-0.30	-0.15	0.00	0.15	0.30	0.45	0.60	0.75
X												
-0.75		11.45	6.49	2.88	2.85	4.24	4.91	4.58	3.26	3.18	6.49	11.72
-0.60		4.55	3.75	2.44	2.24	2.51	2.76	2.72	2.54	2.82	4.27	5.60
-0.45		1.21	1.53	1.48	1.53	1.71	1.84	1.90	1.85	1.98	2.27	2.41
-0.30		-0.09	0.36	0.61	0.80	0.94	1.08	1.07	1.08	1.11	1.16	1.11
-0.15		-0.51	-0.24	-0.01	0.22	0.40	0.51	0.50	0.47	0.39	0.32	0.34
0.00		-0.75	-0.64	-0.44	-0.21	-0.05	0.00	0.01	-0.10	-0.20	-0.31	-0.27
0.15		-0.94	-0.82	-0.63	-0.42	-0.29	-0.24	-0.33	-0.45	-0.68	-0.85	-0.94
0.30		-1.12	-0.85	-0.63	-0.48	-0.40	-0.40	-0.53	-0.70	-0.92	-1.25	-1.61
0.45		-0.85	-0.48	-0.38	-0.32	-0.31	-0.34	-0.47	-0.69	-0.99	-1.35	-1.90
0.60		0.48	0.58	0.29	0.11	0.09	0.03	-0.19	-0.49	-0.70	-0.84	-1.25
0.75		4.33	2.78	0.93	0.56	0.75	0.81	0.47	-0.12	-0.22	0.51	1.38
$Z=0,$ X		-0.75	-0.60	-0.45	-0.30	-0.15	0.00	0.15	0.30	0.45	0.60	0.75
Y												
-0.30		-6.85	5.12	4.64	2.82	1.84	1.41	1.62	2.50	4.20	4.50	-7.59
-0.15		8.72	5.55	3.67	2.06	1.11	0.73	0.99	1.94	3.38	5.30	7.12
0.00		23.09	7.61	3.09	1.32	0.41	0.00	0.22	1.16	2.91	6.80	23.18
0.15		-0.26	2.45	1.61	0.54	-0.23	-0.54	-0.23	0.41	1.66	2.82	1.20
0.30		-10.49	0.94	0.75	-0.42	-0.97	-1.09	-0.97	-0.41	0.81	1.32	-9.64
0.45		25.90	8.11	1.21	-0.59	-0.52	-0.21	-0.50	-0.64	1.09	8.04	23.36
0.60		50.04	6.95	-3.01	-2.27	0.32	1.35	0.43	-2.39	-3.48	5.53	47.36
0.75		2.83	-19.32	-14.00	-3.96	3.73	6.72	3.70	-4.39	-14.14	-19.81	1.40
$X=0,$ Y					-0.30	-0.15	0.00	0.15	0.30	0.45	0.60	0.75
Z												
0.75					3.32	4.07	4.59	3.89	2.89	1.27	-1.15	-4.70
-0.60					0.00	-1.10	1.30	0.77	-0.22	-2.03	-4.51	-7.86
-0.45					-0.96	0.04	0.28	-0.26	-1.19	-3.01	-5.54	-8.89
-0.30					-1.21	-0.21	0.08	-0.42	-1.47	-3.26	-5.66	-8.96
-0.15					-1.23	-0.23	0.05	-0.52	-1.44	-3.26	-5.64	-8.85
0.00					-1.25	-0.22	0.00	-0.50	-1.41	-3.19	-5.58	-8.75
0.15					-1.23	-0.22	0.00	-0.51	-1.31	-3.11	-5.49	-8.62
0.30					-1.11	-0.08	0.13	-0.36	-1.21	-2.96	-5.24	-8.53
0.45					-0.48	0.50	0.82	0.27	-0.58	-2.29	-4.62	-7.88
0.60					1.50	2.70	3.05	2.64	1.67	0.12	-2.45	-5.67
0.75					7.24	8.23	9.58	9.01	7.47	6.11	3.37	-0.08

of the measured values from the theoretical ones is clearly seen because of the higher scale than in 12b and 12c. The measured inhomogeneity increases in the negative direction (the compensating field is higher) when moving from the origin on the z-axis and on the negative y-axis. This is probably caused by the reinforced concrete in the ceiling and the floor which are very close to both x-coil pairs and penetrated by the magnetic flux. The measured inhomogeneity of the field generated by the y-coil set and z-coil set on the planes $y = 0$ cm and $z = 0$ cm, respectively, follows well the theoretical values (Figs. 12b and 12c).

The inhomogeneity values presented in Fig. 12 describe the off-diagonal component of the field gradient with changing baseline. It was also examined how good the field homogeneity is in the direction of the field vector along the main axis. Table 5 shows the inhomogeneity in a plane along the main axis of each coil set. When compared to Table 3 where the theoretical inhomogeneity values are presented it can be seen that the measured values are 2 - 50 times higher at the distance 15 cm from the origin.

5. ACTIVE AC COMPENSATION SYSTEM

5.1. Requirements for the AC compensation

The active compensation of an alternating magnetic field needs a transducer which can accurately detect the variations of the field, and a control unit to keep the effect of the ambient field as small as possible. How well the compensation system can eliminate noise at a given frequency depends on the sensitivity of the transducer on that frequency.

There exist three alternative transducer types: a fluxgate magnetometer, an induction coil magnetometer and a SQUID magnetometer. All of them have advantages and disadvantages. The choice of transducer sets the ultimate limit to the frequency range to be compensated for. The bandwidth of a fluxgate magnetometer starts from DC but its upper cut-off frequency of a few hundred hertz is smaller than that of an induction coil. For a SQUID magnetometer the usable frequency range is from DC to several kilohertz. The sensitivity of the fluxgate magnetometer for DC and low-frequency fields is of the order of 1 nT. The induction coil magnetometer does not respond to DC at all. However, the sensitivity of the induction coil magnetometer increases as inversely proportional to the frequency and the sensitivity below $1 \text{ nT}_{\text{rms}}/\text{Hz}^{1/2}$ can be obtained on frequencies above 10 Hz. The sensitivity of the SQUID magnetometer is of the order of $20 \text{ fT}_{\text{rms}}/\text{Hz}^{1/2}$ down to frequencies of the order of 1 Hz, where the 1/f-noise starts to increase.

Many research groups have used active AC compensation methods based on the fluxgate magnetometers as transducers [Kel 82, Blo 65, Ros 69]. The attenuation they have obtained on the frequency range from DC to about 1 Hz are of the order of 20 dB. In the active compensation system of the Otaniemi magnetically shielded room the best demonstrated value for the shielding improvement is 50 at 0.1 Hz [Kel 82].

Williamson's group has obtained good results in reducing the low-frequency noise by a cancellation technique [Rom 82]. They used two second-order SQUID gradiometers separated by the distance of 30 m. The signal of the reference gradiometer was used for the cancellation of the noise from the signal of the measurement gradiometer. The low-frequency noise was reduced by about an order of magnitude.

We constructed an AC compensation system in which induction coil transducers were used. The purpose was to study the AC compensation on a wide frequency range, from a few herz to 50 Hz.

5.2. Transducer coils

The transducer coil has to fulfill the condition that the magnetic flux going through the coil divided by its area is the same as the magnetic flux density in the origin of the compensation coil set. The size of the transducer coil can be solved according to Eq. (10) from the following equation

$$\sum_{i=1}^4 N_i \frac{\mu I a_i b_i}{\pi} \left[\frac{a_i^2 + b_i^2 + 2z_i^2}{(a_i^2 + b_i^2 + z_i^2)^{1/2} (a_i^2 + z_i^2)(b_i^2 + z_i^2)} \right] = \frac{1}{4cd} \int_{-c}^c \int_{-d}^d \frac{\mu I}{4\pi} \sum_{j=1}^4 N_j \sum_{i=1}^4 (-1)^i \frac{r_i(x_i + y_i) + x_i^2 + y_i^2}{r_i(r_i + x_i)(r_i + y_i)} dx dy. \quad (11)$$

On the left side of the equation there is the magnetic flux density, which is formed by the compensation coil set (four coils) to its center. On the right side there is the z-component of the flux density produced by the compensation coil set to the point P(x,y,z), where z is constant. It is integrated over the area of the assumed transducer coil and then divided by the coil's area (sides 2c and 2d). This equation gives the size of the transducer coil at a certain distance (z) from the origin. Because the equation has two unknowns, c and d, an initial condition must be set for the ratio c/d.

Although the eddy current effect of the shield was neglected in the calculations, the physical dimensions of the shield must be considered. The walls of the shield determine the minimum distance from the origin to the transducer. In x-, y- and z-directions the minimum distance is 95cm, 58cm and 95 cm, respectively. The size of the transducer coils were computed for each direction according to these dimensions. The shape of the coil was fixed as square. In the x-direction on the plane x = 100 cm the side of the square was computed to be 75cm. In the y-direction on the plane y = -65 cm the corresponding value for the side was 70cm. Figure 13 shows the isoflux density lines and the shape of the computed transducer coil at the plane y = -65 cm. The isoflux density lines are presented as a difference ΔB_i to the flux density in the origin according to the following equation

$$\Delta B_i = \frac{B_i(x, y, z) - B_i(0, 0, 0)}{B_i(0, 0, 0)}, \quad (12)$$

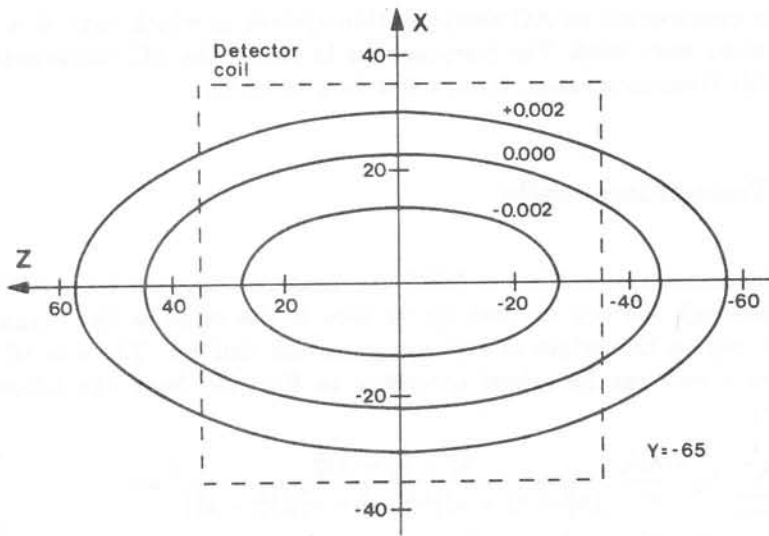


Figure 13. Isoflux density lines $\Delta B_y = -0.002, 0.000$ and $+0.002$ in the plane $y = -65$ cm. The dashed line describes the dimensions of the rectangular coil calculated for this plane. Coordinates given in cm.

where $B_i(x, y, z)$ is the magnetic flux density produced by the compensation coil set i (x, y or z) at the point (x, y, z) in the direction i .

In the z -direction the side of the square was computed to be 100cm. However, this value was considered to be too great because of the limited space in the laboratory and the difficulties in construction as well. A more suitable solution was to construct two smaller circular coils, which were located symmetrically in relation to the z -axis and on the line where $\Delta B_x = 0$. The location of the transducer coil is not necessarily the optimal for the compensation according to the theoretical calculations, because the effect of the ferromagnetic materials in the building is not taken into consideration.

5.3. Alternating field compensator

The ambient alternating magnetic noise can be eliminated by using feeding current to the compensation coil set, which forms a magnetic field opposite to the noise field. A control system is formed by the transducer coil, the alternating field compensator and the compensation coil set. This is presented in Fig. 14 as a block diagram. Electrical connections have been presented by continuous lines and magnetic couplings by broken lines.

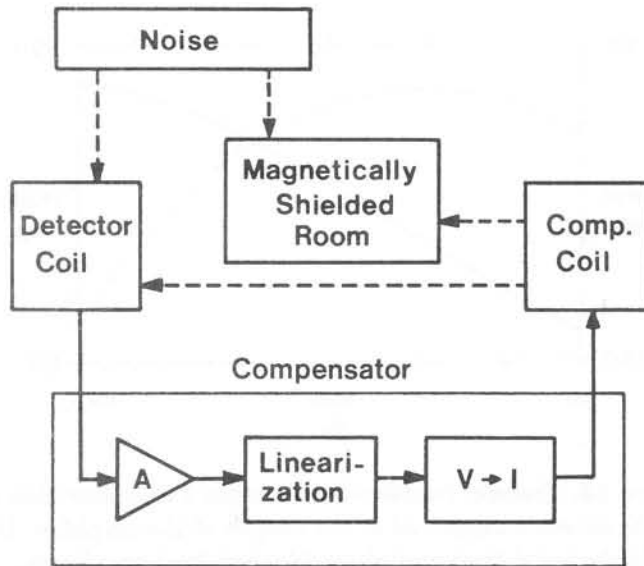


Figure 14. Block diagram of the AC compensation system.

The ambient noise and the field produced by the compensation coil set are summarized and this signal is fed from the transducer to the compensator circuit. This signal is proportional to the magnetic field inside the shield, in the origin, if the requirements for the location and size of the transducer are fulfilled and the source of the ambient noise field is so far away that its field distribution is similar inside the shield and inside the transducer coil.

The amplifier A (Fig. 14) amplifies the transducer signal, after which it is linearized. The object of the linearization is to maintain the phase difference in the feedback loop (transducer-compensator-compensation coil) as 180° on the frequency range to be compensated for. After the linearization the voltage signal is converted to current.

The voltage signal from the transducer coil is not directly proportional to the magnetic flux going through it but ideally to the derivative of the flux. In reality the signal is affected by the resistance and the inductance of the coil and the capacitance between the coil wires as well. Figure 15 presents a measured transfer function between the current fed into the compensation coils and the voltage got from the transducer coil in the x-direction after amplification.

The linearization circuit is based on a double integrator structure. In addition two resistors, R_2 and R_5 (Fig. 16) have been added to achieve a

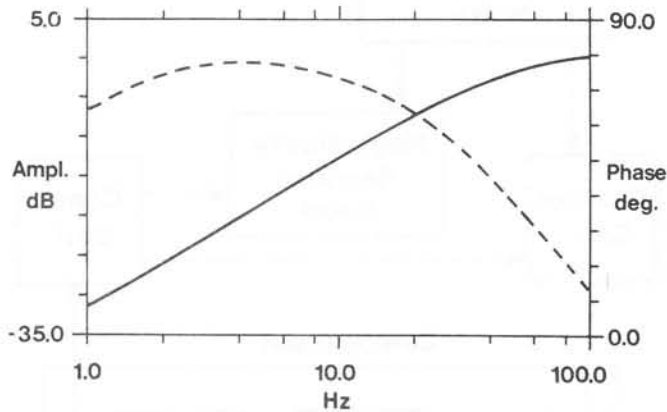


Figure 15. Transfer function between the x-compensation coil and the detector measured at the output of the amplifier. Both amplitude (solid line) and phase (dashed line) are shown.

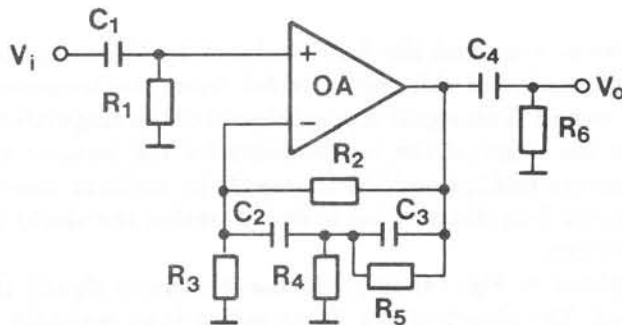


Figure 16. Linearization circuit.

desired transfer function. In the input and the output there are highpass filters to prevent the coupling of $1/f$ -noise and the offset voltage to the output of the compensator. Fig. 17 presents the transfer function measured between the current fed into the compensation coil set and the voltage got after amplification and linearization from the transducer coil.

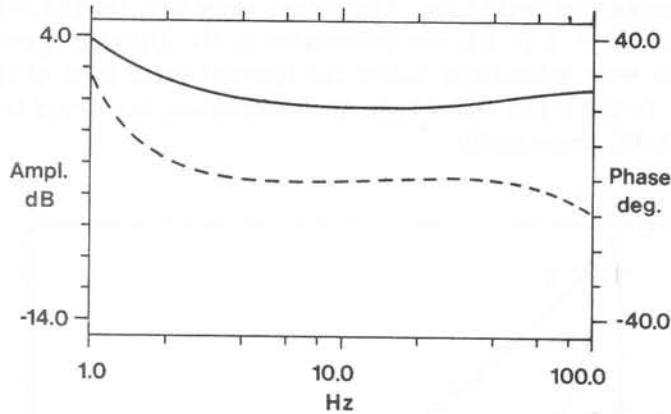


Figure 17. Transfer function between the x-compensation coil and the detector measured after linearization circuit.

5.4. Performance of the AC compensation system

To test the properties of the alternating field compensator an artificial magnetic noise source was used. The noise was created by feeding current to a coil with 10 turns and 60 cm diameter. The coil was situated at 10 m distance from the shield on the next floor. The amplitude of the current was 2.7 A and its frequency was swept continuously from 0.05 Hz to 50 Hz. The noise caused by this source was measured inside the shielded room with and without the AC compensation. The measured spectral densities in the y-direction are shown in Fig. 18. The compensator attenuates by about 15 dB the noise above 8 Hz. However, because of the internal noise of the magnetometer; reliable information about the attenuation at the higher frequency range can not be obtained.

In the x-direction the attenuation of the compensator was negligible at 18 Hz. This verifies that the coupling of the homogeneous noise and of the compensating magnetic field to the chamber is different. If this is not considered, the attenuation of the compensator is 6 dB at the frequency range from 5 Hz to 50 Hz. In the z-direction the attenuation was found to be 12 dB in the range from 10 Hz to 30 Hz.

The effect of the compensation was also tested on a normal working day without any artificial noise. The results show that for the y-direction the noise spike at 6.15 Hz was attenuated 9 dB. Other magnetic noise components were attenuated below the internal noise level of the magnetometer. In the x- and z-directions the attenuation was found to be only 2 dB and 3 dB, respectively.

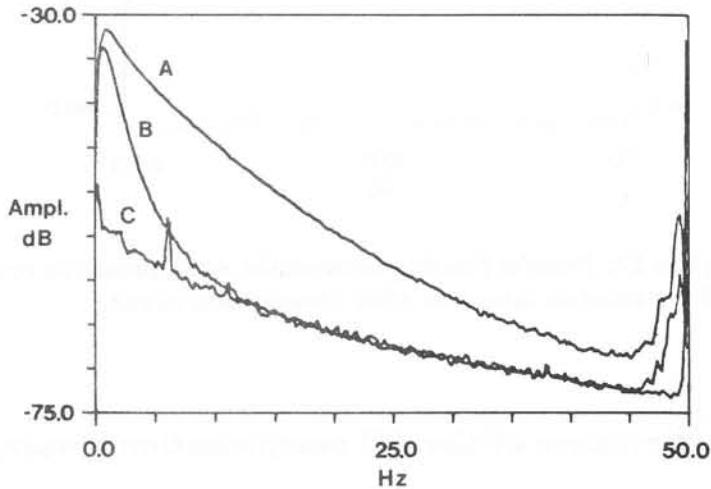


Figure 18. Spectral density of the magnetic flux density measured inside the magnetically shielded room by using an induction coil magnetometer and an artificial noise source when (A) the active AC compensation was not used, (B) when the compensation was used and (C) when the background noise was measured without compensation.

6. PERFORMANCE OF THE TAMPERE MAGNETICALLY SHIELDED ROOM IN BIOMAGNETIC EXPERIMENTS

In the first measurements the movement of the shield on its rubber dampers forced by the ejection of the blood from the subject's heart into the aorta induced strong spurious signals, which distorted the real magnetocardiogram. Thus the additional floor without any contact to the room was a real success. After that relatively good magnetocardiograms could be measured by using a single channel induction coil magnetometer [Lek 81b, Est 82]. Also the three components of the magnetic field vector of the heart were measured the first time simultaneously in our magnetically shielded room by using the induction coil technique [Lek 81a]. These measurements showed that the shield was well suited for magnetocardiography.

The background noise level in the shield was measured with an induction coil magnetometer to be of the order of $40 f T_{rms} / Hz^{1/2}$, and this was verified later with a SQUID magnetometer, Fig. 19. The low-frequency noise increases below the frequency in the order of a few hertz. Although

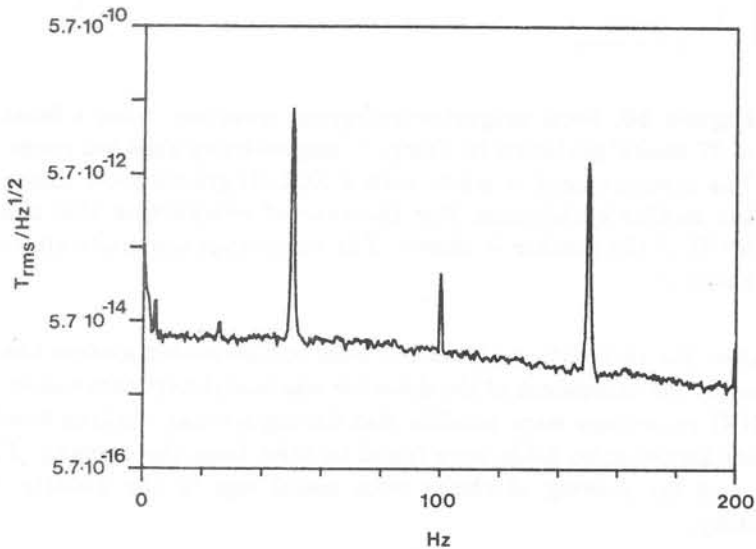


Figure 19. Magnetic background noise level in Tampere magnetically shielded room. The measurement is made with a SQUID gradiometer.

the shield was equipped with pneumatic dampers, the vibration of the building could be seen at some frequencies (Fig. 5). The intensity of the low-frequency noise increased during the day-time when compared to the noise level in the evening and at night. This was caused by the magnetic interferences from different sources and also the increase of the low-frequency vibration and movements of objects in the environment.

After working hours it was possible to obtain a good quality MCG with a SQUID magnetometer. Also some fetal magnetocardiography recordings were made successfully with a balanced SQUID gradiometer, Fig. 20 [Lek 82]. Because of the open door-way the RF-interferences were occasionally a problem. These were eliminated with a thin ($10\ \mu\text{m}$) aluminium foil inside the Dewar around the detection coil.

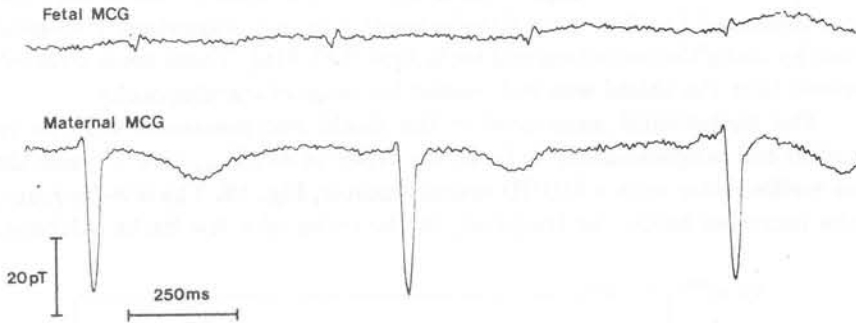


Figure 20. Fetal magnetocardiogram measured from a fetus of 37 weeks' gestation in Tampere magnetically shielded room. The measurement is made with a SQUID gradiometer above the mother's abdomen. For the sake of comparison also the MCG of the mother is shown. The recordings are made alternatively.

After the installation of the DC field compensation system the noise induced by the movement of the detector was completely eliminated. Then the MCG recordings were possible also during normal working hours and the only higher noise fields were found to arise from the opening of metal doors and the moving of chairs with metal legs in the vicinity of the laboratory.

Figure 21 shows an example of a real time measurement of a magnetic heart vector (MHV) taken during a normal working day with a multiplexed SQUID vector magnetometer in the shield [Lek 84]. The active DC compensation was used during the measurement. The subject was a normal 28 year-old male.

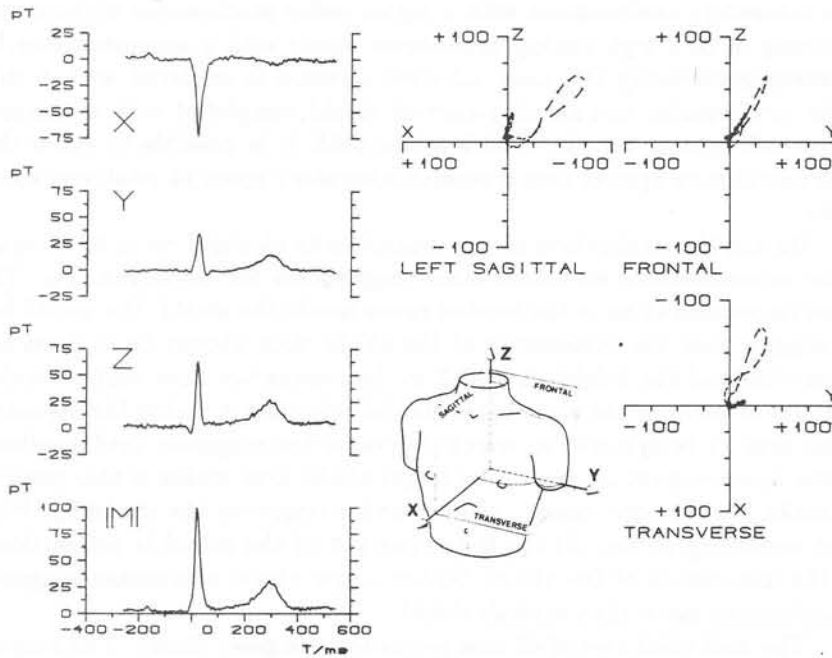


Figure 21. Real time recording of the magnetic heart vector with a multiplexed SQUID vector magnetometer in Tampere magnetically shielded room. The subject is 28 year-old normal male.

7. DISCUSSION

It is generally known that technically and economically most efficient noise rejection is not achieved by using only one noise rejection method but with the simultaneous application of various noise rejection techniques. This means that, though it is possible to measure the magnetocardiogram in a laboratory environment with a higher order gradiometer without any shielding or in a high quality multi-layer shield with a magnetometer, in vectormagnetometry the most effective solution is achieved with a first order gradiometer and an eddy-current shield completed with a compensation coil system for the earth's static field. It is possible to build this instrumentation system into a normal laboratory room at relatively small costs.

During the application of our magnetically shielded room to biomagnetic measurements we found some suggestions for improvements. The most important thing is the limited space inside the shield. We would like to suggest that the dimensions of the shield floor should be at least say $2.5\text{m} \times 3\text{m}$ and the height about 2.2 m. Increasing the floor surface makes it easier to perform the measurements. Additionally it makes the measurement area more symmetric, which decreases the magnetic field gradients in the measurement location. The larger shield area makes it also possible to make the corridor longer, which further improves the shielding. Note that according to Eq. (2) the time constant of the shield is proportional to the dimensions of the shield. So the larger shield attenuates magnetic interferences more than a small shield.

The wall thickness of 45 mm seems to be a good choice. The suspension system works satisfactorily. There have been also other solutions by other research groups for damping and vibration [Ber 81, Kel 82]. The selection of the damping principle depends on the properties of the building.

The homogeneity of our compensation coil system is probably better than that of the earth's magnetic field, which is distorted by the ferromagnetic material of the building. However, we recommend the construction used in our coil system because it is very practical to construct and fits well in the laboratory room.

If one wants to spend more money on the instrumentation system, we suggest that it should be spent on more effective AC compensation of the magnetic interference and good filtering of the signal. We have applied digital line-frequency filtering with good results [Hei 84]. Another filtering method also is adaptive filtering, which gives better results in a changing noise environment.

8. SUMMARY

An eddy current shield equipped with an active compensation system to cancel the static and low-frequency magnetic field has been constructed. Its shielding properties and performance in biomagnetic experiments have been thoroughly examined.

The required shielding factor can be determined according to the existing laboratory noise, which depends on the laboratory location. The ultimate limit for the shielding is the noise level of the detector. Also the use of a differential magnetometer decreases the needed shielding factor.

Our eddy current shield is constructed from 45 mm thick aluminium plate and its outer dimensions are $2\text{m} \times 2\text{m} \times 2\text{m}$. The doorway is made as a corridor and no closed door is used. The shield is equipped with pneumatic dampers and a plywood floor without any contact to the shield. The attenuation of the shield for a 50 Hz magnetic field is measured to be 44 dB, 46 dB and 50 dB in the x-, y- and z-direction, respectively.

The compensation for the static field of the earth is important because of the induced noise generated by the vibration of the detector in the DC field. In cardiac studies the changes in the intracardiac blood volume generate a susceptibility signal when there exists a magnetic field. It can be eliminated when the magnetic field is compensated for.

In our compensation coil system the vertical or x-component of the magnetic field is compensated for with four coaxial square coils in two planes. The y- and z-components are each compensated for with four coaxial rectangular coils in four planes. The dimensions of the x-coils have been solved according to the method of *Kakuno* and *Gondo* and the dimensions of the rectangular coils in the y- and z-directions experimentally on the basis of the square coil solution.

Three independent current sources have been constructed for the compensation. The current feeding system is based on power MOSFETs and the negative feedback loop which keeps the current stable. The adjustments can be made with an accuracy of $100 \mu\text{A}$ in the y- and z-channels and of $200 \mu\text{A}$ in the x-channel. The current feeding system is protected against high connection transients. The drift of the compensation currents after an hour's warmup time causes a drift of the order of 4.8 nT in the total magnetic flux density. The line frequency ripple in the DC current is at maximum $32 \mu\text{A}$.

The field distribution of the DC compensation coil set has been

measured with a fluxgate magnetometer. The feeding current was a square wave current of 0.05 Hz. The effect of the low-frequency magnetic fluctuations was avoided with this method. The magnetic flux density components were measured at a total of 968 points inside the shield during the magnetically silent periods of the day. The results show that the inhomogeneity distribution of the compensation field agrees well with the theoretical values except in the x-direction where the field homogeneity is distorted possibly by the ferromagnetic material in the ceiling and floor.

An active AC compensation system for frequencies from a few hertz to 50 Hz has been tested. The noise field is detected by using relatively large induction coils. The dimensions of the transducer coils have been determined according to the field distribution of the compensation coil set outside the shield. The control system to eliminate the noise field is formed by the transducer coil, the alternating field compensator and the compensation coil set. By using an artificial magnetic noise source the maximum attenuation of 6 dB, 15 dB and 12 dB was obtained for the x-, y- and z-directions, respectively. However, for the normal existing magnetic noise the attenuation was found to be below 10 dB for the y-direction and 2 dB and 3dB for the x- and z-directions, respectively.

REFERENCES

- [Ber 81] Bercy, C., Duret, D., Karp, P. and Teszner, D., Installation of a biomagnetic measurement facility in a hospital environment. *Biomagnetism. Proceedings Third International Workshop on Biomagnetism*, Berlin (West) (1981), p. 95-106.
- [Blo 65] Bloom, A.L., Innes, D.J., Rempel, R.C. and Ruddock, K.A., Octagonal coil system for canceling the earth's magnetic field. *J. Appl. Phys.* **36**(1965)8, p. 2560-2565.
- [Bre 69] Brechna, H., Pair of current loops. *Methods of Experimental Physics, Vol. 8*, Problems and solutions for students. Eds. L. Morton and W.F. Hornyak. Academic Press, New York and London, 1969.
- [Coh 67] Cohen, D., Enhancement of ferromagnetic shielding against low-frequency magnetic fields. *Appl. Phys. Lett.* **27**(1967), p. 67-69.
- [Ern 81] Erné, S.N., Hahlbohm, H.-D., Scheer, H. and Trontelj, Z., The Berlin magnetically shielded room (BMSR), Section B - Performances. *Biomagnetism. Proceedings Third International Workshop on Biomagnetism*, Berlin (West) (1981), p. 79-87.
- [Fre 67] Freedman, M.S., Wagner, F.Jr., Porter, F.T. and Day, P., Large volume degausser with gradient compensation. *J. Appl. Phys.* **38**(1967)4, p. 1856-1862.
- [Hei 80] Heinonen, P., Tuomola, M., Leikkala, J. and Malmivuo, J., Properties of a thick-walled conducting enclosure in low-frequency magnetic shielding. *J. Phys. E: Sci. Instrum.* **13**(1980), p. 569-570.
- [Hei 84] Heinonen, P., Saramäki, T., Malmivuo, J. and Neuvo, Y., Periodic interference rejection using coherent sampling and waveform estimation. *IEEE Trans. Circ. Syst. CAS-* **31**(1984)5, p. 438-446.
- [Kak 76] Kakuno, K. and Gondo, Y., Three and four square coil systems for producing uniform magnetic fields. *Bulletin of the faculty of engineering*, Yokohama National Univ. **25**(1976), p. 179-192.
- [Kat 82] Katila, T., Maniewski, R., Tuomisto, T., Varpula, T. and

- Siltanen, P., Magnetic measurement of cardiac volume changes. *IEEE Trans. Biomed. Eng.* **BME-29**(1982)1, p. 16-25.
- [Kel 82] Kelh , V.O., Pukki, J.M., Peltonen, R.S., Penttinen, A.J., Ilmoniemi, R.J. and Heino, J.J., Design, construction, and performance of a large-volume magnetic shield. *IEEE Trans. Mag.* **MAG-18**(1982)1, p. 260-270.
- [Lek 81a] Lekkala, J. and Malmivuo, J., Simultaneous measurement of the magnetic heart vector components with unipositional lead system. *Biomagnetism. Proceedings Third International Workshop on Biomagnetism.* Berlin (West) (1981), p. 475-484.
- [Lek 81b] Lekkala, J.O. and Malmivuo, J.A.V., Noise reduction using a matching input transformer. *J. Phys. E: Sci. Instrum.* **14**(1981), p. 939-942.
- [Lek 82] Lekkala, J. and Malmivuo, J., SQUID-vectormagnetometer for biomagnetic research. *Proc. of World Congress on Medical Physics and Biomedical Engineering 1982.* Ed. Bleifeld, W., Harder, D., Leetz, H.-K. and Schaldach, M., Hamburg, September 5-11, 1982.
- [Lek 84] Lekkala, J. and Malmivuo, J., Multiplexed SQUID vectormagnetometer for biomagnetic research. *J. Phys. E: Sci. Instrum.* **17**(1984)6, p. 504-512.
- [Mag 81] Mager, A., The Berlin magnetically shielded room (BMSR), Section A: Design and construction. *Biomagnetism. Proceedings Third International Workshop on Biomagnetism,* Berlin (West) (1981), p. 51-78.
- [Mal 81] Malmivuo, J., Heinonen, P., Tuomola, M. and Lekkala, J., Thick-walled conducting shield in biomagnetic experiments. *Biomagnetism. Proceedings Third International Workshop on Biomagnetism,* Berlin (West) (1981), p. 107-112.
- [Pit 63] Pittman, M.E. and Waidelich, D.L., Three and four coil systems for homogeneous magnetic fields. *Trans. IEEE* **36**(1963)1, p. 36-45.
- [Rom 82] Romani, G.L., Williamson, S.J. and Kaufman, L., Biomagnetic instrumentation. *Rev. Sci. Instrum.* **53**(1982), p. 1815-1845.
- [Ros 69] Ross, K.J. and Garment, R., An arrangement for servomechanically controlled Helmholtz-coils. *J. Phys. E: Sci. Instrum.* **2**(1969)5, p. 437.
- [Saf 67] Safonov, Y., Provotorov, V., Lub , V. and Yakimenkov,

- L., Method of recording the magnetic field of the heart (magnetocardiography). *Bull. Exp. Biol. Med.* **64**(1967), p. 1022-1024.
- [Str 81] Stroink, G., Blackford, B., Brown, B. and Horacek, M., Aluminium shielded room for biomagnetic measurements. *Rev. Sci. Instrum.* **52**(1981)3, p. 463-468.
- [Web 54] Weber, E., *Electromagnetic fields. Theory and applications. Volume I - Mapping of fields.* New York, John Wiley & Sons, 1954.
- [Wik 75] Wikswo, J.P., Malmivuo, J.A.V., Barry, W.H., Grawford, G.E., Fairbank, W.M., Giffard, R.P., Harrison, D.C. and Roy, R.H., Vectormagnetocardiography - An improved technique for observation of the electrical activity of the human heart. *Proc. San Diego Biomed. Symposium*, **14**(1975), p. 359-367.
- [Wil 81] Williamson, S.J. and Kaufman, L., Magnetic fields of the cerebral cortex. *Biomagnetism. Proceedings Third International Workshop on Biomagnetism*, Berlin (West) (1981), p. 353-402.
- [Zim 77] Zimmerman, J.E., SQUID instruments and shielding for low-level magnetic measurements. *J. Appl. Phys.* **48**(1977), p. 702-710.